1994

Competing C–Br and C–C Bond Fission Following 1[n(O),π*(C=O)] Excitation in Bromoacetone: Conformation Dependence of Nonadiabaticity at a Conical Intersection

P. W. Kash

G.C.G. Waschewsky

R. E. Morss

L. J. Butler

Michelle M. Francl
Bryn Mawr College, mfrancl@brynmawr.edu

Custom Citation
P.W. Kash, G.C.G. Waschewsky, R.E. Morss, L.J. Butler, M.M. Francl. *J. Chem. Phys.* **100** (5), 3463 (1994).

Competing C–Br and C–C bond fission following $^1[n(O),\pi^*(C{=}O)]$ excitation in bromoacetone: Conformation dependence of nonadiabaticity at a conical intersection

P. W. Kash, G. C. G. Waschewsky, R. E. Morss, and L. J. Butler
The James Franck Institute and Department of Chemistry, The University of Chicago, Chicago, Illinois 60637

M. M. Francl
Department of Chemistry, Bryn Mawr College, Bryn Mawr, Pennsylvania 19010

(Received 26 July 1993; accepted 24 November 1993)

These experiments investigate the competition between C–C and C–Br bond fission in bromoacetone excited in the $^1[n(O),\pi^*(C{=}O)]$ absorption, elucidating the role of molecular conformation in influencing the probability of adiabatically traversing the conical intersection along the C–C fission reaction coordinate. In the first part of the paper, measurement of the photofragment velocity and angular distributions with a crossed laser-molecular beam time-of-flight technique identifies the primary photofragmentation channels at 308 nm. The time-of-flight spectra evidence two dissociation channels, C–Br fission and fission of one of the two C–C bonds, BrH_2C–$COCH_3$. The distribution of relative kinetic energies imparted to the C–Br fission and C–C fission fragments show dissociation is not occurring via internal conversion to the ground electronic state and allow us to identify these channels in the closely related systems of bromoacetyl- and bromopropionyl chloride. In the second part of the work we focus on the marked conformation dependence to the branching between C–C fission and C–Br fission. Photofragment angular distribution measurements show that C–Br fission occurs primarily from the minor, *anti*, conformer, giving a β of 0.8, so C–C fission must dominate the competition in the *gauche* conformer. Noting that the dynamics of these two bond fission pathways are expected to be strongly influenced by nonadiabatic recrossing of the reaction barriers, we investigate the possible mechanisms for the conformation dependence of the nonadiabatic recrossing with low-level *ab initio* electronic structure calculations on the C–Br reaction coordinate and qualitative consideration of the conical intersection along the C–C reaction coordinate. The resulting model proposes that C–C bond fission cannot compete with C–Br fission in the *anti* conformer because the dissociation samples regions of the phase space near the conical intersection along the C–C fission reaction coordinate, where nonadiabaticity inhibits C–C fission, while from the *gauche* conformer C–C fission can proceed more adiabatically and dominate C–Br fission. A final experiment confirms that the branching ratio changes with the relative conformer populations in accord with this model.

I. INTRODUCTION

Predictive models for the branching between chemical reaction pathways often rely on statistical transition state theories[1–4] or quantum scattering calculations[5] on a single adiabatic potential energy surface. The potential energy surface gives the energetic barriers to each chemical reaction and allows prediction of the reaction rates. Yet the reaction dynamics evolves on a single potential energy surface only if the Born–Oppenheimer[6] separation of nuclear and electronic motion is valid. Recent work[7,8] has shown that the breakdown of the Born–Oppenheimer approximation at a reaction barrier formed from an avoided electronic configuration crossing[9] can dramatically reduce the rate constant for the chemical reaction and change the resulting branching between energetically allowed product channels.

The qualitative mechanism for the reduction in the reaction rate due to nonadiabatic recrossing of the barrier is illustrated in Fig. 1 for an A–B bond fission reaction with a barrier along the forward and reverse reaction coordinates. Along the adiabatic reaction coordinate the dominant electronic configuration changes from one bonding in the A–B bond, on the reactant side of the barrier, to one repulsive in the A–B bond, after the barrier in the exit channel region. The change in electronic wave function required to follow the adiabatic reaction coordinate near the barrier is considerable, and can result in a failure of the Born–Oppenheimer approximation. If the splitting between the adiabatic electronic surfaces at the barrier along the reaction coordinate is small, reflecting the weak configuration interaction between the bonding and repulsive electronic configurations, the molecule may not traverse the barrier adiabatically. Instead the electronic wave function may retain the bonding configuration character, resulting in a nonadiabatic hop to the upper bound potential energy surface at the avoided crossing. The molecule feels the bound wall of that potential instead of undergoing bond fission on the lower adiabat. The reduction in rate due to nonadiabatic recrossing of the reaction barrier is considerable for reactions in which the splitting between

 0021-9606/94/100(5)/3463/13/$6.00

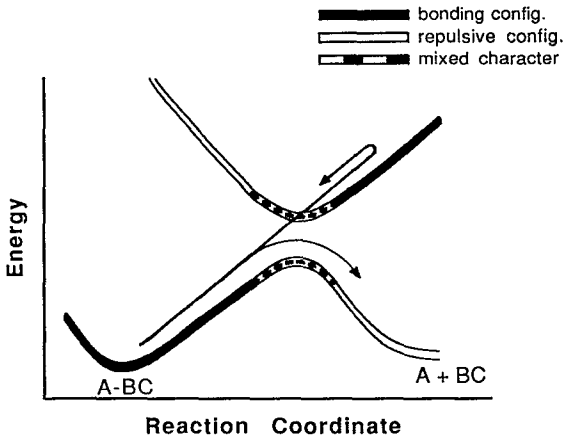

FIG. 1. Schematic reaction coordinate for the A−BC→A+BC reaction with a barrier to both the forward and reverse reaction. Along the lower adiabat, the dominant electronic configuration of the electronic wave function changes from bonding in character on the reactant side to repulsive (antibonding) in character on the product side. The figure also shows the upper bound adiabat formed from the avoided electronic crossing of the bonding and repulsive electronic configurations. If the Born–Oppenheimer approximation fails, the molecule retains its initial bonding electronic character at the barrier and makes a nonadiabatic "hop" to the upper adiabat instead of proceeding to products on the lower adiabat.

adiabats is small,[10] notably for Woodward–Hoffmann forbidden reactions[8] and reactions with a conical intersection along the reaction coordinate.

Our previous work on the 248 nm photodissociation of bromoacetyl[7] and bromopropionyl chloride,[8] where the splitting between adiabats at the barrier to both C–Cl and C–Br bond fission is relatively small, examined the distance dependence of the configuration interaction matrix elements at the barrier to C–Br fission. In bromoacetyl chloride, the initial $^1n(O)\pi^*(C{=}O)$ electronic transition results in a C–Cl:C–Br bond fission ratio of 1.0:0.4, while in bromopropionyl chloride the same initial transition results in a C–Cl:C–Br bond fission ratio of 1.0: < 0.05. Increasing the distance between the C=O and C–Br chromophores by inserting a single CH_2 spacer decreased the electron correlation between the $n(O)\pi^*(C{=}O)$ configuration initially excited and the $n(Br)\sigma^*(C{-}Br)$ configuration necessary for C–Br bond fission. Consequently, the splitting between the adiabats at the avoided crossing of the $n(O)\pi^*(C{=}O)$ configuration and the $n(Br)\sigma^*(C{-}Br)$ configuration is much smaller in bromopropionyl chloride than in bromoacetyl chloride, resulting in over an order of magnitude reduction in the branching to C–Br fission due to nonadiabatic recrossing of the reaction barrier.

The present work on bromoacetone examines the competition between bond fission channels belonging to two classes of reactions highly susceptible to nonadiabatic effects; C–Br fission on the $^1A''$ potential energy surface is Woodward-Hoffmann forbidden and fission of the C–C bond proceeds through a conical intersection. The earlier part of the paper focuses on experimentally determining the primary product channels upon $^1n(O)\pi^*(C{=}O)$ excitation at 308 nm. The second part, in Secs. V A–V C, investigates the marked dependence of the nonadiabatic branching on molecular conformation. We present a model in which nonadiabatic recrossing of the barrier to C–C fission reaction depends strongly on molecular conformer, proposing that the *anti* conformer accesses regions of the conical intersection where the splitting between adiabats is very small, while the *gauche* conformer accesses regions where C–C fission can proceed adiabatically and dominate C–Br fission. To test the model, a final measurement examines if altering the *gauche:anti* ratio in the parent molecules changes the relative branching between C–C and C–Br bond fission in accord with the model's prediction.

II. EXPERIMENTAL METHOD

To measure the photofragment velocities and angular distributions from the photodissociation of bromoacetone, $BrCH_2COCH_3$, we use a crossed laser-molecular beam apparatus.[11,12] Upon photodissociation with a pulsed excimer laser, neutral dissociation products scatter from the crossing point of the laser and the molecular beam with velocities determined by the vector sum of the molecular beam velocity and the recoil velocity imparted in the dissociation. Those scattered into the acceptance angle of the differentially pumped detector travel 44.1 cm to an electron bombardment ionizer and are ionized by 200 eV electrons. After mass selection with a quadrupole mass filter, the ions are counted with a Daly detector and multichannel scalar with respect to their time-of-flight (TOF) from the interaction region after the dissociating laser pulse. Upon subtraction of the calibrated ion flight time, forward convolution fitting of the TOF spectrum determines the distribution of energies imparted to relative product translation in the dissociation. The angular distribution of the scattered photofragments is obtained with a linearly polarized photolysis beam by measuring the variation in signal intensity with the direction of the electric vector of the laser in the molecular beam/detector scattering plane.

The molecular beam was formed by expanding gaseous bromoacetone, at its vapor pressure at 40 °C, seeded in He to give a total stagnation pressure of 300 torr. The 0.076 mm diameter nozzle was heated to roughly 180 °C in the measurements of the angular distribution of the primary photofragments. The peak beam velocity was 1.28×10^5 cm/s with a full-width-at-half-maximum of 13%. In addition, the nozzle was heated to either 100 °C or 400 °C in the measurements to determine the changes in the relative branching between primary C–Br and C–C bond fission as a function of the *anti:gauche* ratio in the parent molecular beam. To measure the velocity of the parent molecular beam *in situ*, the molecular beam source was rotated to point into the detector and a chopper wheel raised into the beam. To measure the velocities of the neutral photofragments, the molecular beam source is rotated to a different angle in the plane containing the beam and detector axis, a plane perpendicular to the laser beam propagation direction. Laser polarization angles and molecular beam source angles are given here with respect to the detector axis, one defined as positive with clockwise rotation and the other as positive with counterclockwise rotation.

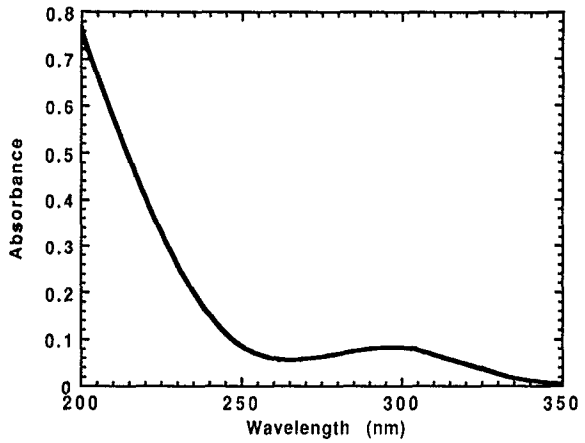

FIG. 2. Ultraviolet absorption spectrum of bromoacetone. The $^1n(O)\pi^*(C{=}O)$ absorption band peaks near 300 nm. The spectra were recorded on a Perkin–Elmer Lambda 6 UV/VIS spectrophotometer at bromoacetone's equilibrium vapor pressure at room temperature with a 1 cm path length.

Time-of-flight and angular distribution measurements were made on bromoacetone photofragments at 308 nm. The source angle was maintained at 15° with respect to the detector axis for the data with a 180 °C nozzle and 10° for the data with a 100 °C and 400 °C nozzle. The unpolarized laser power from a Questek 2640 excimer was typically 100 mJ/pulse, with the light focused to a 5 mm^2 spot size at the crossing region of the laser and molecular beam. Polarized spectra typically were taken at 21 mJ/pulse. Quadrupole resolution was adjusted to 1.7 amu FWHM for $m/e^+=79$ (Br^+) and to 0.6 amu for $m/e^+=43$ (CH_3CO^+) and $m/e^+=42$ (CH_2CO^+). For the anisotropy measurements, we disperse the unpolarized laser light into two linearly polarized components with a single crystal quartz Pellin–Broca and use the horizontal component, rotating the polarization into the desired direction with a half-wave retarder. The polarization dependent signal, integrated in many repeated short scans and alternating between each laser polarization direction, required no additional normalization to laser power or detector efficiency.

Signal was observed at several parent and daughter ions of the neutral primary photofragments. The strong signal observed at Br^+ after 100 000 shots evidences primary C–Br fission. The weaker signal at CH_2CO^+ and CH_3CO^+ after 200 000 shots evidence primary C–C bond fission in addition to momentum matching the Br^+ signal. In addition, small signal is detected at $BrCH_2^+$ and CH_3^+. No signal was detected at $CH_2COCH_3^+$ after 200 000 shots. Nor was there signal at HBr^+ or CH_3Br^+ after 300 000 shots.

III. COMPUTATIONAL METHOD

To help interpret the experimental results, we also present *ab initio* electronic structure calculations for bromoacetone using the GAUSSIAN 92 system of programs[13] with an STO-3G* basis set. Configuration interaction with single and double excitations (CISD) calculations provide electronic ground state energies in the harmonic region of the C–Br and C=O stretching potentials. These energies in the harmonic region are then fit to a Morse oscillator with the correct dissociation energy. The ground state energy, as a function of the C–Br and C=O stretching coordinates, is then assumed to be a sum of two independent Morse oscillators. Configuration interaction with single excitations (CIS) calculations provide excitation energies from the ground electronic state to the relevant excited electronic states. These CIS excitation energies are added to the ground state Morse oscillator energies to construct the excited electronic state surfaces. Calculation of the excited electronic states provides the relative barrier height to C–Br bond fission along the lowest adiabatic excited electronic state for both the *gauche* and *anti* conformer. In addition, the calculations also provide energetic splittings between the two lowest adiabatic excited electronic states at the avoided crossing in the C–Br bond fission channel for both conformers. Because the $^1n(O)\pi^*(C{=}O)$, excited electronic state, accessed by a 308 nm photon, has a longer C=O bond length than in the ground electronic state, we present CIS calculations of the avoided crossing region on the excited electronic surfaces at a variety of C=O bond lengths which represent the range of C=O stretching motion likely sampled by the dissociative wave function.

IV. IDENTIFICATION OF PRIMARY PRODUCT CHANNELS: C–Br AND C–C BOND FISSION

When bromoacetone is excited at 308 nm in the $^1[n(O),\pi^*(C{=}O)]$ absorption band[14] (see Fig. 2), the C–Br bond, β to the carbonyl group, and the C–C α bond break. Figure 3 shows the photofragment TOF spectra taken at $m/e^+=79$, Br^+, with 100 000 laser shots and a 180 °C nozzle. All of the signal was attributed to primary C–Br fission:

$$BrCH_2COCH_3+h\nu(308\ \text{nm})\rightarrow Br+CH_2COCH_3. \quad (1)$$

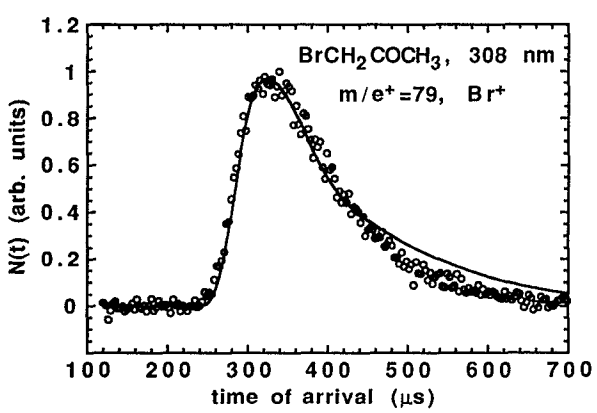

FIG. 3. Laboratory time-of-flight spectrum of the photofragments detected at Br^+ from bromoacetone photodissociated at 308 nm with an unpolarized laser. The source angle was 15°. All of the signal results from primary C–Br bond fission and is fit with a $P(E_T)$ shown in Fig. 4.

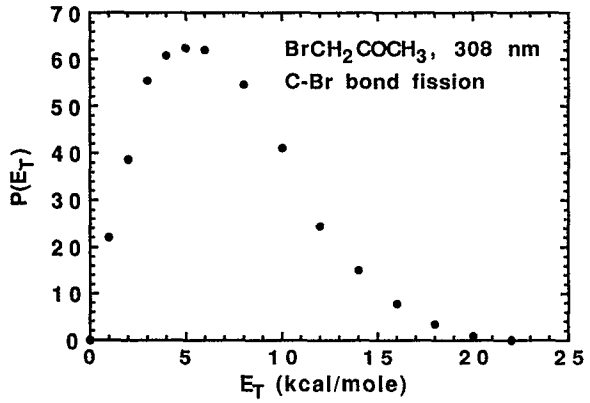

FIG. 4. The center-of-mass product translational energy distribution, $P(E_T)$, for the C–Br bond fission channel in bromoacetone at 308 nm. The $P(E_T)$ is derived from forward convolution fitting the Br^+ signal in Fig. 3.

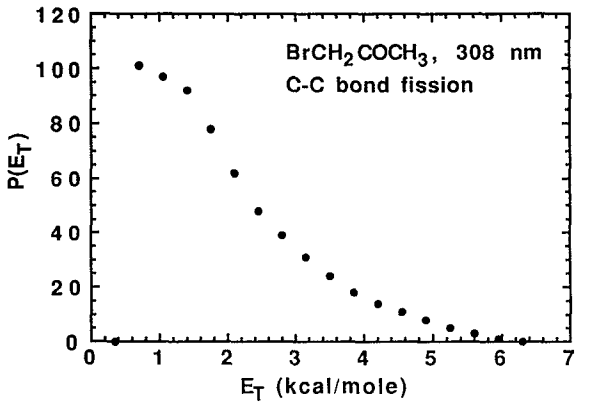

FIG. 6. The center-of-mass product translational energy distribution, $P(E_T)$, for the C–C bond fission channel in bromoacetone at 308 nm. The $P(E_T)$ is derived from forward convolution fitting the CH_3CO^+ signal which results from primary C–C bond fission in Fig. 5.

Through forward convolution fitting of the Br spectra, a center-of-mass (c.m.) translational energy distribution, $P(E_T)$, (Fig. 4) which peaks near 5 kcal/mol was derived for C–Br bond fission. Figure 5 shows the photofragment TOF spectra taken at $m/e^+=43$, $COCH_3^+$, with 200 000 laser shots and a 180 °C nozzle. All of the signal except for the fastest edge was attributed to primary C–C bond fission:

$$BrCH_2COCH_3+h\nu(308\ nm)\rightarrow BrCH_2+COCH_3. \quad (2)$$

The portion of the $COCH_3^+$ spectra attributed to primary C–C bond fission gave a translational energy distribution (Fig. 6) peaking near very low energies but extending out near 5 kcal/mol or approximately one-third of the 15 kcal/mol available energy. This distribution for primary C–C bond fission was used to fit the small signal detected at $m/e^+=93$, $BrCH_2^+$, shown in Fig. 7, showing the required momentum match between fragments. In addition, the TOF spectra shown in Fig. 8, taken at $m/e=42$, $COCH_2^+$ with a 180 °C nozzle, shows significant contributions from both the C–Br and the C–C bond fission channels.The fast component of the $COCH_2^+$ spectra, peaking near 280 μs, which was fit with the translational energy distribution for primary C–Br fission shown in Fig. 4, results from primary CH_2COCH_3 fragments cracking in the ionizer to give $COCH_2^+$ daughter ions. Similarly, the slow component in the $COCH_2^+$ spectra peaking near 350 μs and fit with the translational energy distribution for primary C–C bond fission shown in Fig. 5, results from primary $COCH_3$ fragments cracking in the ionizer to $COCH_2^+$ daughter ions. Finally, the TOF spectra taken at $m/e^+=15$, CH_3^+ (Fig. 9), also shows contributions from both primary C–Br and C–C bond fission. Although the signal to noise in the CH_3^+ TOF spectra is poor, the data is fit rather well by assuming that both the CH_2COCH_3 products, which result from primary C–Br bond fission and have a translational energy

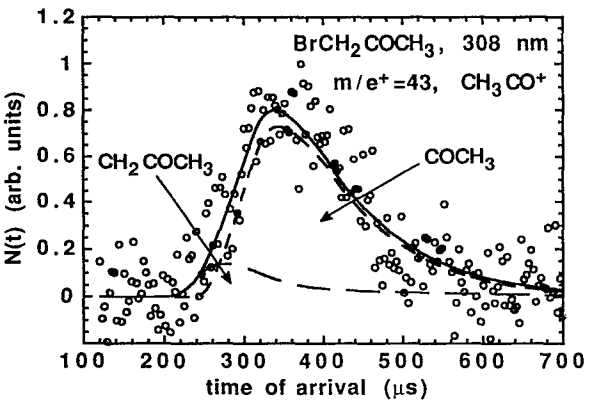

FIG. 5. Laboratory time-of-flight spectrum of the photofragments detected at CH_3CO^+ from bromoacetone photodissociated at 308 nm with an unpolarized laser. The source angle was 15°. The contribution from CH_2COCH_3 fragments to the CH_3CO^+ spectrum was determined by fitting the signal with the $P(E_T)$ in Fig. 4 derived from forward convolution fitting the Br^+ signal. The rest of the signal results from the CH_3CO fragments produced in primary C–C bond fission and is fit with the $P(E_T)$ in Fig. 6.

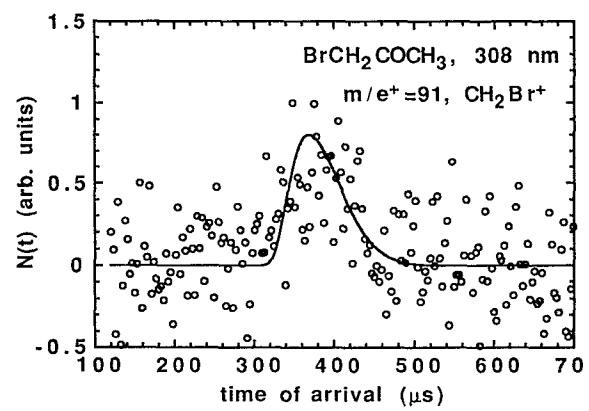

FIG. 7. Laboratory time-of-flight spectrum of the photofragments detected at CH_2Br^+ from bromoacetone photodissociated at 308 nm with an unpolarized laser. The source angle was 15°. The signal is fit with the $P(E_T)$ for primary C–C bond fission in Fig. 6, showing the required momentum match between the CH_2Br and $COCH_3$ partners resulting from C–C bond fission.

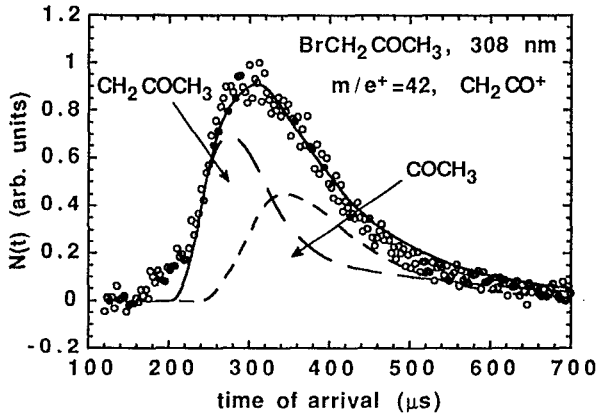

FIG. 8. Laboratory time-of-flight spectrum of the photofragments detected at CH_2CO^+ from bromoacetone photodissociated at 308 nm. The nozzle temperature was 180 °C and the source angle was 15°. The contribution from CH_2COCH_3 fragments to the CH_2CO^+ signal was determined by fitting the signal with the $P(E_T)$ for primary C–Br bond fission in Fig. 4. Similarly, the contribution from $COCH_3$ fragments to the spectrum was determined by fitting the signal with the $P(E_T)$ for primary C–C bond fission shown in Fig. 6.

distribution shown in Fig. 4, and the $COCH_3$ fragments, which result from primary C–C bond fission and have a translational energy distribution shown in Fig. 6, crack to CH_3^+ ions in the ionizer. Thus, all the signal observed in the TOF spectra could be fit by just two primary bond fission channels using the kinetic energy distributions in Figs. 4 and 6.

The kinetic energy distributions of the C–Br and the C–C bond fission products both evidence significant probability for dissociation events imparting several kilocalories to relative product translation. This indicates that, for both channels, dissociation does not proceed via a mechanism involving internal conversion to the ground electronic state, but rather via a reaction coordinate that has a significant exit barrier (barrier to reverse reaction) so the fragments exert a repulsive force on each other as they separate. The data indicate that for C–Br fission, the mechanism is similar to that for C–Br fission in bromoacetyl chloride upon excitation in the $^1[n(O),\pi^*(C{=}O)]$ absorption, which occurs on a $^1A''$ potential energy surface resulting from the avoided electronic crossing of the $^1n(O)\pi^*(C{=}O)$ and the $n(Br)\sigma^*(C\text{–}Br)$ configurations and has a substantial exit barrier. Indeed, we have used the bromoacetone C–Br $P(E_T)$ to separate this source of C–Br fission product in bromoacetyl chloride from that resulting from an overlapping repulsive electronic transition in that molecule.[8,15]

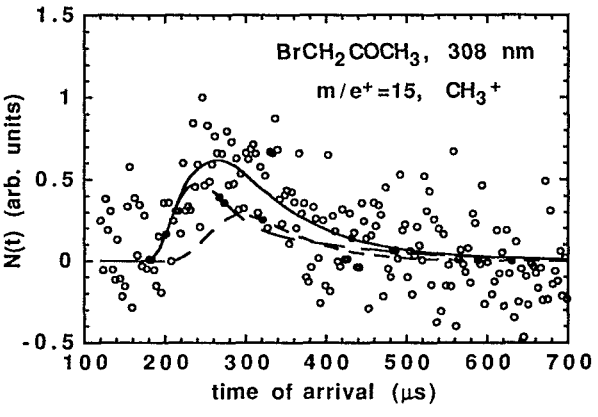

FIG. 9. Laboratory time-of-flight spectrum of the photofragments detected at CH_3^+ from bromoacetone photodissociated at 308 nm. The source angle was 15°. Although the signal is rather noisy, the data is approximately fit assuming contributions form both C–C and C–Br bond fission. The contribution from CH_2COCH_3 fragments to the CH_3^+ signal was determined by fitting the signal with the $P(E_T)$ for primary C–Br bond fission in Fig. 4. Similarly, the contribution from $COCH_3$ fragments to the spectrum was determined by fitting the signal with the $P(E_T)$ for primary C–C bond fission shown in Fig. 6.

The observation of C–C fission in bromoacetone was also of considerable interest, as we had not identified any C–C fission products in bromoacetyl chloride. This led us to search for a contribution from C–C fission in the previous data. Reference 16 analyzes the previous bromoacetyl chloride data assuming any C–C fission would impart the same distribution of relative kinetic energies to C–C fission products as that observed in Fig. 6 from bromoacetone. The usefulness of this approximation was supported by our results on bromopropionyl chloride,[8] where a forward convolution fit using the $P(E_T)$ from the bromoacetone data to predict the arrival time of C–C bond fission product exactly corresponded to a shoulder in the Br^+ TOF spectrum (from detection of $BrCH_2CH_2$ at the Br^+ daughter ion). Reanalysis[16] of the previous bromoacetyl chloride data using the $P(E_T)$ for C–C bond fission determined here for bromoacetone does indeed show that a small portion of the Br^+ signal likely results from CH_2Br fragments from C–C fission. Although this in no way alters the major conclusions from this previous work, it does slightly alter the $P(E_T)$ derived for C–Br fission and the previously reported C–Cl:C–Br branching ratio from bromoacetyl chloride as detailed in Ref. 16.

V. CONFORMATION DEPENDENCE OF THE COMPETITION BETWEEN C–C AND C–Br FISSION IN BROMOACETONE

This section presents perhaps the most exciting results of this work, the marked conformation dependence of the C–C:C–Br fission branching ratio. In Sec. V A below we first present a surprising result: The angular distribution of C–Br fission products shows C–Br fission occurs predominantly only from the *anti* conformer. (To be consistent with previous authors, we retain the nonstandard designation of *anti* for the bromoacetone conformer where the Br atom is, in fact, *s-cis* to the O atom.[17]) The next two sections analyze what factors result in the molecule undergoing significant branching to C–Br fission in the *anti* conformer but not in the *gauche* conformer. Because the C–Br:C–C branching ratio for each conformer is equal to the ratio of the individual bond fission rate constants, $k_{C\text{–}Br}/k_{C\text{–}C}$, a larger branching to C–Br fission from the *anti* conformer can result from either an increased rate constant for C–Br fission in the *anti* conformer or a decreased rate constant for C–C fission. Thus, we analyze the

potential conformation dependence of each reaction channel to understand the conformational dependence of the branching. Section V B presents *ab initio* calculations on the reaction coordinate for C–Br fission. They show the rate constant for C–Br fission should be larger in the *gauche* conformer than in the *anti* conformer, not smaller, so the conformation dependence of the branching cannot be understood by only considering the conformation dependence of the C–Br reaction coordinate; one must consider the C–C fission reaction coordinate. Section V C details the potential impact of molecular conformer on the competing C–C fission channel. Simple consideration of molecular symmetry suggests that in the *anti* conformer C–C bond fission should sample the reaction coordinate near the conical intersection, where C–C fission is suppressed due to nonadiabatic recrossing of the reaction barrier, but the *gauche* conformer accesses regions of the conical intersection where C–C fission could proceed adiabatically. The last section tests the model by measuring the change in the C–Br:C–C branching ratio induced by changing the *anti:gauche* population ratio in the molecular beam.

A. Data suggestive of conformational control of C–C:C–Br branching: The angular distribution of the C–Br fission products

The first hint of the influence of molecular conformation on the competition between C–C and C–Br fission in bromoacetone came out in the comparison of the measured and predicted photofragment angular distributions. Below we analyze the angular distributions of the $COCH_3$ fragments from C–C fission and the Br atoms from C–Br fission of bromoacetone at 308 nm. The data shows that dissociation is prompt with respect to molecular rotation, but that the C–Br fission products result primarily from the *anti* conformer.

Figure 10 shows the integrated $COCH_3$ fragment signal from C–C bond fission vs Θ_{LAB}, the angle between the laser electric vector and the detector axis. The best fit to the photofragment angular distribution is obtained by varying the anisotropy parameter, β, in the classical electric dipole expression[18]

$$\omega(\theta_{c.m.}) = (1/4\pi)[1+\beta P_2(\cos\theta_{c.m.})]. \quad (3)$$

Because $\theta_{c.m.}$ is the angle between the recoil direction of the photofragment in the center-of-mass frame and the electric vector of the light in the laboratory frame, fitting the data involves converting between the c.m. and lab frame using the measured molecular beam velocity and the $P(E_T)$ derived from the unpolarized data. The forward convolution fit of the data showed the photofragment anisotropy for C–C bond fission to be parallel with $\beta=0.7$. The anisotropic angular distribution shows that C–C bond fission is fast with respect to molecular rotation. Furthermore, we can predict what the anisotropy parameter would be if the transition moment were the same as that for the $^1[n(O),\pi^*(C{=}O)]$ transition in formaldehyde and bromoacetyl chloride in the limit that photofragment recoil is axial, along the C–C bond direction, and prompt with respect to molecular rotation. Taking the $^1[n(O),\pi^*(C{=}O)]$ transition moment as in the C–C=O plane and perpendicular to the C=O bond axis, the angle between the C–C bond and the orientation of the transition dipole moment is[19] $\alpha=32.6°$ in the ground electronic state, giving a predicted anisotropy parameter[20] of $\beta=2P_2(\cos\alpha)=1.12$. Thus both the observed and predicted angular distribution are highly parallel. The slightly less anisotropic distribution measured experimentally could result from either moderate rotational smearing or a distortion of the molecular frame in the excited state which changed the direction of the C–C axis by only 9°, as an α of 41° can reproduce the observed anisotropy of 0.7. Thus the close correspondence between the observed and predicted values of β confirms the orientation of the $^1[n(O),\pi^*(C{=}O)]$ transition dipole moment in bromoacetone.

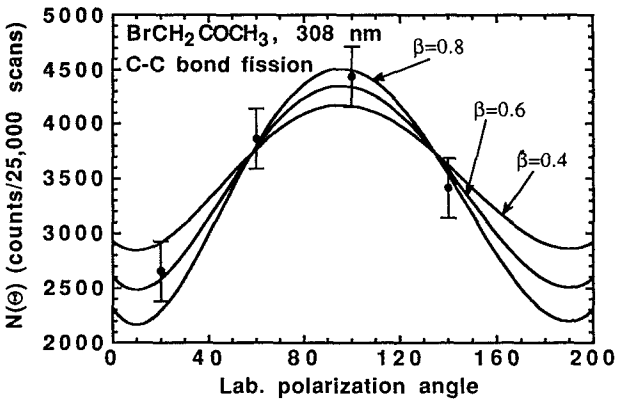

FIG. 10. Laboratory angular distributions of the CH_3CO^+ signal which results from primary C–C bond fission in bromoacetone photodissociated at 308 nm with linearly polarized light. Θ is the angle of the laser electric vector with respect to the detector axis (measured in the opposite sense of rotation as the source angle). The data points represent the integrated experimental TOF signal measured at four different laser polarization angles. Each data point represents signal integrated between 351 and 525 μs corresponding to laboratory velocities of 8.0×10^4 to 14.0×10^4 cm/s. Line fits show the predicted change in detected scattered signal intensity with laser polarization angle obtained, after transformation from the center of mass to laboratory frame, with three trial anisotropy parameters, $\beta=0.8$, $\beta=0.6$, and $\beta=0.4$.

Using the same orientation of the transition moment and molecular geometry, we can also try to predict the angular distribution of the Br atoms from C–Br bond fission and compare it to the experimental result. Because the angle between the transition moment and the C–Br bond is different in the two thermally populated molecular conformers, we expect the angular distribution will reflect a weighted average of the two individual angular distributions. In the *anti* conformer, the 32.1° angle between the C–Br axis[19] and the direction of the electronic transition dipole moment gives a predicted $\beta_{anti}=2P_2(\cos 32.1°)=1.15$, while in the *gauche* conformer the predicted anisotropy is $\beta_{gauche}=2P_2(\cos 73.05°)=-0.75$. The *gauche* conformer is calculated to be more stable than the *anti* by 0.5 kcal/mol,[19] so using this energy difference and assuming no conformational cooling in the expansion,[21] the experimental nozzle temperature of 180 °C gives 77.8%

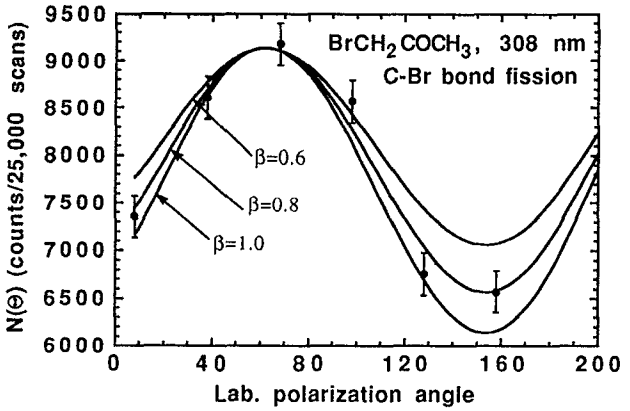

FIG. 11. Laboratory angular distributions of the Br^+ signal which results from primary C–Br bond fission in bromoacetone photodissociated at 308 nm with linearly polarized light. Θ is the angle of the laser electric vector with respect to the detector axis (measured in the opposite sense of rotation as the source angle). Each data point represents the integrated experimental TOF signal measured at six different laser polarization angles. The data points represented signal integrated between 255 and 717 μs corresponding to laboratory velocities of 8.55×10^4 to 23.15×10^4 cm/s. Line fits show the predicted change in detected scattered signal intensity with laser polarization angle obtained, after transformation from the center of mass to laboratory frame, with three trial anisotropy parameters, $\beta=1.0$, $\beta=0.8$, and $\beta=0.6$.

gauche and 22.2% *anti* in the molecular beam. Weighting the predicted β values for the *gauche* and *anti* conformers by their relative populations gives a predicted $\beta=22.2\%(1.15)+77.8\%(-0.75)=-0.33$ for comparison with the experimental data.

If the C–Br:C–C fission branching ratio were the same for both conformers, we expect that the angular distribution of the Br atom fragments would be well predicted by the average anisotropy parameter calculated above.[22] Figure 11 shows the integrated Br signal vs θ_{LAB}. The best fit to the Br photofragment angular distribution gave $\beta=0.8$, in sharp contrast to the conformation weighted prediction of -0.33. Clearly, the *gauche* and *anti* conformers do not contribute at all equally to C–Br fission. Indeed, the predicted value of $\beta=1.15$ for the *anti* conformer alone agrees much better with the experimentally determined β value, particularly if there is a small amount of smearing of the distribution due to rotation or distortion of the molecular frame in the excited state as presumed for C–C fission. In the limiting case, to be consistent with the measured anisotropy at most 18% of the C–Br bond fission events result from *gauche* bromoacetone even though 78% of the molecules are in the *gauche* conformer. Thus, although we observe both C–C and C–Br fission in bromoacetone, it is apparent that C–Br fission can dominate C–C fission in the *anti* conformer, but not in the *gauche*.

B. Developing a model for the conformation dependence of C–Br:C–C branching: C–C fission through a conical intersection

To develop a model for understanding why C–Br fission could dominate C–C fission in the *anti*, but not in the *gauche*, conformer we first examine the possible influence of molecular conformation on the C–Br fission reaction coordinate, then we turn to the C–C fission reaction coordinate. Part 2 outlines a model in which the nonadiabatic recrossing probability for C–C fission through a conical intersection depends strongly on molecular conformation. The following section details a final experiment to test whether the branching ratio changes with the relative conformer populations in accord with this proposed model.

1. Ab initio investigation of the possible influence of conformation on the C–Br fission reaction coordinate

Because our previous work on the related systems of bromoacetyl- and bromopropionyl chloride had shown that the branching to C–Br fission could be greatly reduced by nonadiabatic recrossing of the reaction barrier on the $^1A''$ excited potential energy surface, we first turned our attention to the conformation dependence of nonadiabatic recrossing along the C–Br reaction coordinate in bromoacetone. We seek to determine which of the two reaction pathways drive the observed conformational dependence of the branching ratio, equal to the ratio of the individual bond fission rate constants, k_{C-Br}/k_{C-C}. The observed increase in the C–Br:C–C branching ratio for the *anti* conformer can result from either an increase in the rate constant for C–Br fission in the *anti* conformer or a decrease in the rate constant for C–C fission. The *ab initio* calculations, described in detail below, show that the rate constant for C–Br fission is smaller, not larger, in *anti*-bromoacetone than in *gauche*-bromoacetone, because nonadiabatic recrossing of the C–Br reaction barrier is less pronounced in the *gauche* conformer. Thus the observed increase in branching to C–Br fission over C–C fission in the *anti* conformer cannot be understood without considering the conformation dependence of the rate constant for C–C fission; this is addressed in Secs. V B 2 and V B 3.

Figure 12 shows cuts along the C–Br stretch coordinate of the calculated singlet excited electronic states of *anti*- (left) and of *gauche*- (right) bromoacetone.[23] Although at this simple level of *ab initio* calculation the barrier energies are too high, the calculations still provide useful qualitative information. The electronic character of the lowest $^1A''$ potential energy surface in the *anti* conformer, as determined by the dominant electronic configuration in the GAUSSIAN 92 output, plainly changes from $n(O)\pi^*(C{=}O)$, (a',a''), in character to $n(Br)\sigma^*(C-Br)$, (a'',a'), in character across the barrier to C–Br fission, as expected for an adiabat resulting from the avoided electronic curve crossing of these two electronic configurations. The lowest repulsive A' surface, characterized by an in plane $n(Br)\sigma^*(C-Br)$ electronic configuration, does not interact with the A'' states so is not shown in the figure. For the *anti* conformer, cuts in the excited state potential energy surface are determined by stretching the C–Br bond while fixing the C=O bond length at 1.182, 1.282, 1.392, and 1.492 Å. Similarly, for *gauche* bromoacetone cuts are taken with the C=O bond length at 1.186, 1.280, 1.380, and 1.480 Å.[24] For the *gauche* conformer, in principle all three of the electronic states can mix and avoid each other,

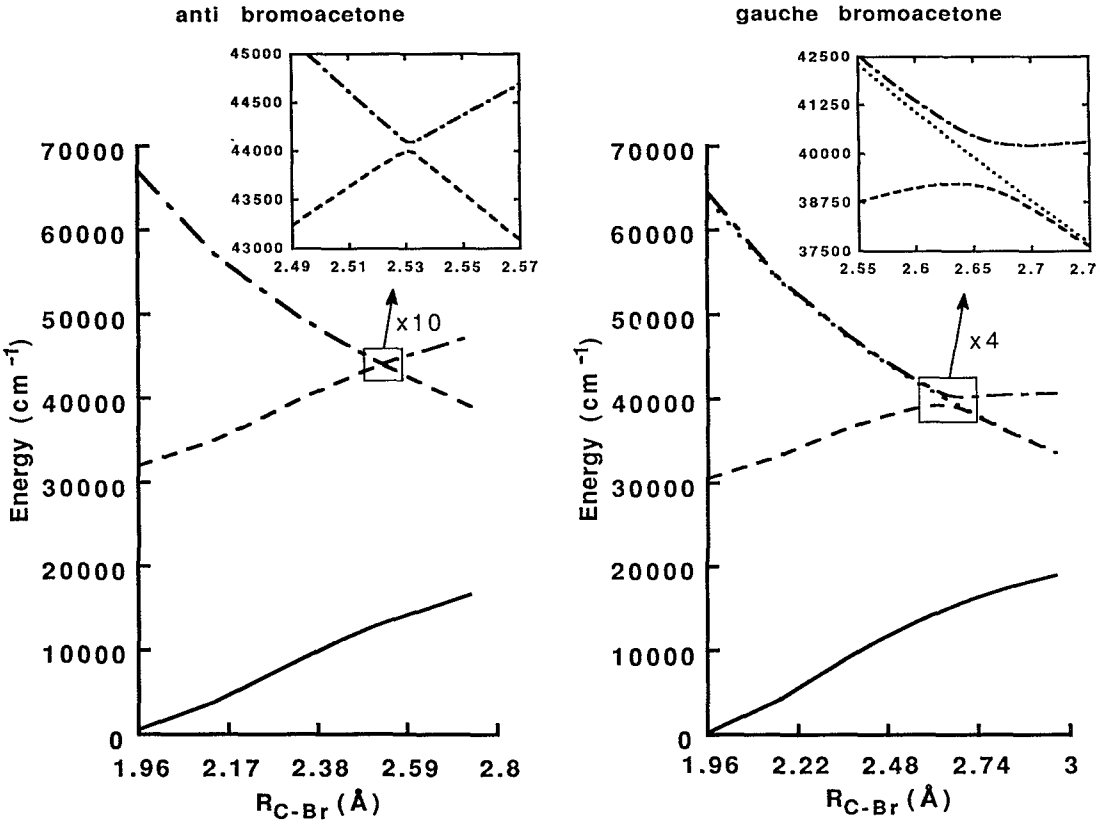

FIG. 12. Cuts through the calculated *ab initio* electronic surfaces for *gauche*-bromoacetone with $R(C{=}O) = 1.280$ Å (right) and *anti*-bromoacetone with $R(C{=}O) = 1.282$ Å (left). Although for the *gauche* conformer all three electronic states can in principle mix and split, it is clear that one of the three states does not interact strongly with the other two. The avoided crossing of the two other states forms the adiabatic reaction coordinate for C–Br fission, just as the avoided crossing of the two $^1A''$ states does in *anti* bromoacetone. The boxed-in portions at the barrier to each bond fission pathway, which are enlarged in the insets above each plot, show that the splitting between adiabats at the barrier to C–Br bond fission in *anti*-bromoacetone is smaller by at least a factor of eight than that in *gauche*-bromoacetone. This smaller splitting between adiabats should contribute to a nonadiabatic suppression of C–Br bond fission in the *anti* conformer, while the experiments show that the C–Br fission occurs almost exclusively from the *anti* conformer. This apparent contradiction suggests that C–C bond fission competes effectively with C–Br fission in the *gauche* conformer (Sec. V B 2). For the particular cuts along the avoided crossing seam shown here, the splitting at the avoided crossing to C–Br fission is 1220 cm^{-1} in *gauche*-bromoacetone and only 97 cm^{-1} in *anti*-bromoacetone. Other cuts are given in Table I.

as none may be strictly characterized with a plane of symmetry. However, Fig. 12 clearly shows that one of the three states does not interact strongly with the other two, while the other two show an avoided curve crossing which forms the adiabatic reaction coordinate for C–Br fission. Thus, in the next paragraph when we analyze the avoided crossing which forms the barrier to C–Br fission, we only consider two interacting electronic states for both *anti*- and *gauche*-bromoacetone.

Because the barrier to C–Br fission is similar in the two conformers, we turn to consider if there is a conformation dependence to the nonadiabatic recrossing of the C–Br bond fission barrier that can explain the observed conformation dependence of the branching ratio. The smaller the energetic splitting, $2V_{12}$, between the two adiabats at the barrier formed from the avoided electronic crossing, the larger the probability that the Born Oppenheimer approximation will fail and result in nonadiabatic recrossing of the transition state, suppressing C–Br fission. Equivalently, in an approximately diabatic representation, if the off-diagonal potential coupling V_{12} between the $n(O)\pi^*(C{=}O)$ bound state and the $n(Br)\sigma^*(C\text{–}Br)$ repulsive state is small, the dynamics will remain on the $n(O)\pi^*(C{=}O)$ bound diabat as the C–Br bond stretches through the curve crossing and return to the Franck–Condon region instead of coupling onto the C–Br repulsive electronic state and cleaving the C–Br bond. Table I summarizes the results of the calculations by showing the energy of the lowest excited electronic state and the splitting between the adiabats [formed from the interacting $^1n(O)\pi^*(C{=}O)$ and $n(Br)\sigma^*(C\text{–}Br)$ configurations] at the point of the avoided crossing in the various one-dimensional cuts which were calculated. For both conformers, the splitting varies along the seam of the avoided crossing; the avoided crossing occurs at longer C–Br bond distances, with an increasingly smaller splitting, for cuts taken at longer C=O distances. However, the energetic splitting at the avoided crossing in the C–Br bond fission channel for the *anti* conformer is, while similar to that in *trans*-bromoacetyl chloride, much smaller (by at least a

TABLE I. Summary of *ab initio* calculations of the splitting between adiabats at the barrier to C–Br bond fission in (a) *anti*- and (b) *gauche*-bromoacetone. The first two columns give the C=O and C–Br bond lengths, in Å, at the barrier. The third column shows the calculated energy at the barrier on the lowest (of A'' symmetry for the *anti*) singlet excited adiabatic electronic surface (referenced to the minimum energy in the ground state). The fourth column, labeled $2V_{12}$, shows the splitting between the two adiabats at the barrier formed from the avoided electronic curve crossing. The coordinates of the barrier were found by freezing the C=O geometry at the numbers given in each row of the table and freezing all the other internuclear coordinates except the C–Br distance at the equilibrium values reported in Ref. 19 for each conformer.

$R_{(C=O)}$(Å)	R(C-Br)(Å) at barrier	Energy (cm^{-1}) at barrier on $1\,^1A''$, referenced to minimum in the ground state	$2V_{12}$ (cm^{-1})
(a)			
1.182	2.39	51131	129
1.282	2.53	44008	97
1.392	2.67	42941	75
1.492	2.77	46503	59
(b)			
1.186	2.51	45808	1982
1.280	2.66	39143	1220
1.380	2.83	37645	720
1.480	3.00	39324	432

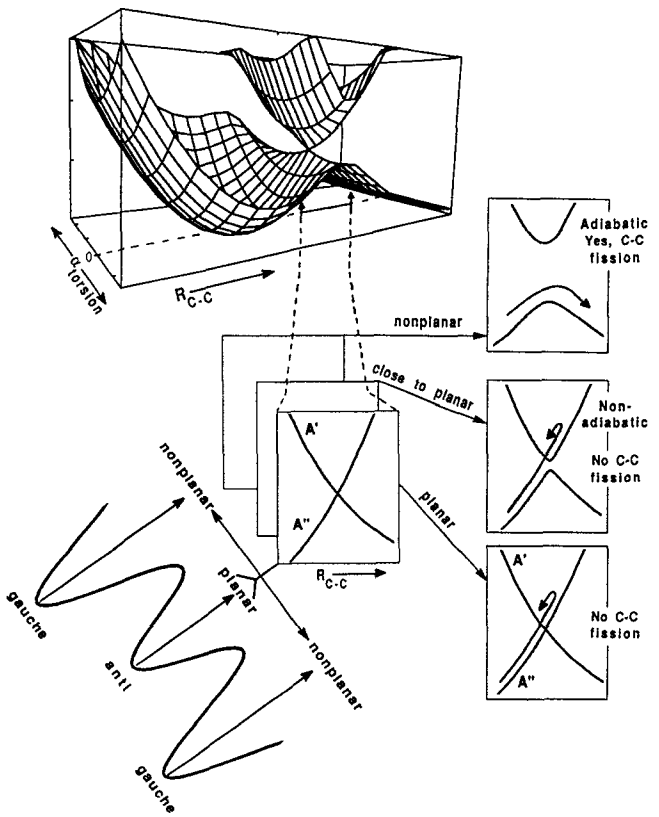

FIG. 13. Schematic representation of the different regions of the conical intersection along the C–C fission reaction coordinate sampled by dissociating the *anti* vs the *gauche* conformer. The frames on the right side of the figure show three slices through the conical intersection: the lowest at planar geometry ($\alpha_{torsion}=0$); the middle at close to planar geometries (small α) where the adiabats are weakly split, so nonadiabatic recrossing dominates the dynamics; and the uppermost at highly nonplanar geometries, sampled by dissociative trajectories from the *gauche* conformer, where the adiabats are strongly split so C–C fission can proceed adiabatically.

factor of seven for the cuts at the four C=O geometries in Table I) than that for *gauche*-bromoacetone, not larger. (This result can be understood qualitatively; the splitting between adiabats is expected to be anomalously small for Woodward–Hoffmann forbidden reactions, but in the *gauche* conformer the reaction is no longer strictly Woodward–Hoffmann forbidden as there is no longer a plane of symmetry.) As a result, any conformation dependence to the branching due to nonadiabaticity along the C–Br fission reaction coordinate would act to suppress C–Br fission in *anti*-bromoacetone much more than in *gauche*-bromoacetone. The experimental results, however, showed that k_{C-Br}/k_{C-C} is larger, not smaller, in the *anti* conformer. Thus the observed increase in the C–Br:C–C branching ratio for the *anti* conformer does not result from an increase in the rate constant for C–Br fission in the *anti* conformer, but rather from a considerable decrease in the rate constant for C–C fission. In other words, the C–Br fission channel dominates C–C fission in the *anti* conformer not because the rate constant for C–Br fission is higher than in the *gauche*, but because the rate constant for C–C fission is much lower in the *anti* than in the *gauche* conformer. The next section carefully considers the C–C fission reaction coordinate to develop a model for understanding the conformation dependence of the branching.

2. The conformation dependence of C–C fission through a conical intersection

The most compelling model for why C–Br fission dominates C–C fission in the *anti* conformer but not in the *gauche* conformer comes from considering the C–C fission reaction coordinate. Armed with the experimental result that C–C fission is occurring on a potential energy surface with an exit barrier, resulting in significant kinetic release to product translation, we note that both on the lowest singlet and the lowest triplet excited electronic state the reaction coordinate for C–C fission is formed from the avoided crossing of the Franck–Condon excited $n(O)\pi^*(C{=}O)$ state and a repulsive $\sigma\sigma^*(C{-}C)$ configuration.[25–28] However, the $n(O)\pi^*(C{=}O)$ configuration has A'' symmetry in C_s while the repulsive $\sigma\sigma^*(C{-}C)$ state has A' symmetry, so the two states interact only at nonplanar[29] geometries, resulting in a conical intersection as shown in Fig. 13. The electronic configuration interaction matrix elements which contribute to V_{12} and couple the $n(O)\pi^*(C{=}O)$ and $\sigma\sigma^*(C{-}C)$ configurations are necessarily zero in C_s symmetry. Likewise, the splitting between the upper and lower adiabats in regions of phase space near the conical intersection is quite small, so any dissociative trajectories which attempt to traverse the conical intersection along the adiabatic C–C fission reaction coordinate in regions of phase space close to planar geometries will not

be able to dissociate, but will rather retain bound $n(O)\pi^*(C{=}O)$ electronic character and return to the Franck–Condon region.

Nonadiabatic recrossing of the C–C fission reaction barrier near the conical intersection, then, provides the best explanation for the observed conformation dependence of the C–Br:C–C branching. If one induces just a slight amount of out-of-plane bending or torsional vibration about the equilibrium geometry of the *anti* conformer during dissociation, the dissociative wave function will sample the conical intersection along the C–C fission reaction coordinate where the splitting between the adiabats is still small, so nonadiabatic recrossing of the barrier should completely suppress C–C fission. C–Br fission can then dominate in the *anti* conformer, giving C–Br fission products with the observed parallel angular distribution. However, if one can induce out-of-plane bending or, equivalently, break the plane of symmetry by inducing torsion about the C–C bond, rotating the Br atom out of the plane of symmetry, the dissociative trajectories could access regions of the conical intersection where the splitting between the adiabats is larger, so C–C fission could proceed adiabatically. Although at our low level of *ab initio* calculation we were not able to calculate the splitting between adiabats as a function of the dihedral angle between the C–Br and C=O groups, (we only know it is zero in the *anti* conformer and nonzero, due to symmetry, in the *gauche*) the analysis presented here of the experimental results thus far indicates that the rate constant for C–C fission is considerably enhanced in the *gauche* conformer. Thus the photodissociation of the *gauche* conformer of bromoacetone must allow Franck–Condon access to dissociative wave functions that traverse the conical intersection at nonplanar geometries where the adiabats avoid each other strongly, so C–C fission proceeds easily, as shown in Fig. 13. The lack of observation of C–Br fission from the *gauche* conformer suggests that once C–C fission can proceed more adiabatically, it dominates C–Br fission. In the next section, we test this model by changing the relative population of *anti* and *gauche* conformers in the beam and determining how the observed branching ratio between C–C and C–Br fission changes.

3. Test of the model: Changing the populations of the molecular conformers to sample different regions of the conical intersection

If C–C fission proceeds predominantly from photoexcitation of the *gauche* conformer, where it can dissociate adiabatically through the conical intersection, and C–Br fission dominates in the *anti* conformer, because the competing C–C fission channel is nonadiabatically suppressed near planar geometries, then we should be able to alter the observed branching ratios by changing the relative populations of *gauche* and *anti* conformers in the molecular beam. Assuming little conformational cooling in the expansion,[21] we can increase the fraction of the higher (by about 0.5 kcal/mol)[19] energy *anti* conformer in the molecular beam by increasing the nozzle temperature. Figure 14 compares the $m/e^+=42$, CH_2CO^+, time-of-arrival spectrum taken at a 100 °C nozzle temperature, where there are significant contributions from both primary C–Br and primary C–C bond fission, with the same spectrum taken at a 400 °C nozzle temperature. The spectra in Fig. 14 show that the increased population of the *anti* conformer at 400 °C results in a decreased contribution to the CH_2CO^+ signal from primary C–C fission relative to the signal from C–Br bond fission. To separately identify the two contributions to the CH_2CO^+ daughter ions' spectrum, we calculate the predicted arrival time spectrum of the $COCH_3$ product of C–C fission and the CH_2COCH_3 product of C–Br fission using the individually measured kinetic energy distributions for C–C and C–Br fission shown in Figs. 6 and 4. We then change the relative probability of each bond fission channel until a good fit to the spectra in Fig. 14, with contributions from both, is achieved. The percentage contribution from each bond fission channel that fit the CH_2CO^+ data are at 100 °C: 78% from primary C–Br bond fission and 22% from primary C–C bond fission, vs that at 400 °C nozzle temperature: 85% from primary C–Br bond fission and 15% from C–C bond fission. These percentages already include corrections for kinematic factors and angular distribution, but must be weighted by the relative ionization cross section for $COCH_3$ and CH_2COCH_3 fragments and the probability of giving CH_2CO^+ daughter ion to obtain absolute C–Br:C–C branching ratios.

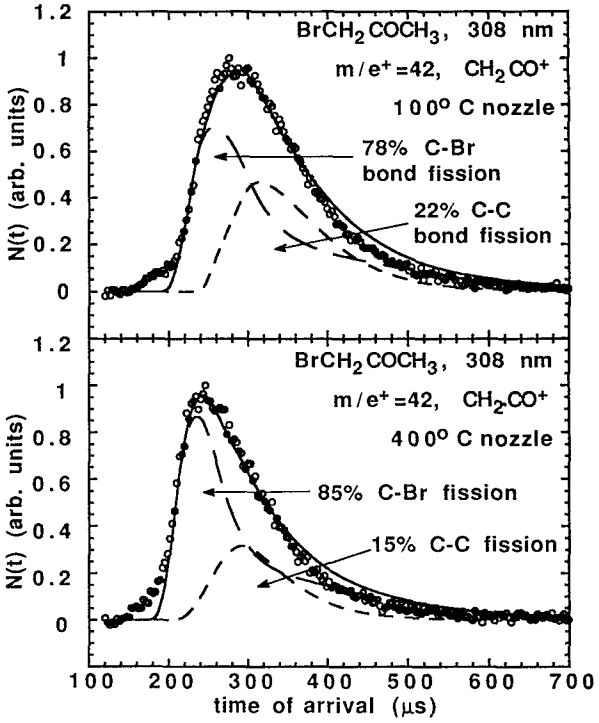

FIG. 14. Laboratory time-of-flight spectra at two nozzle temperatures of the photofragments detected at CH_2CO^+ from bromoacetone photodissociated at 308 nm. Top: With a nozzle temperature of 100 °C. Bottom: With a nozzle temperature of 400 °C. The source angle was 10° for both spectra.

Although this data does not give an absolute

C–Br:C–C fission branching ratio at each conformational temperature because the daughter ion cracking patterns of CH_2COCH_3 and $COCH_3$ are unknown, we can obtain a precise measure of the relative branching ratio change and compare it directly to the relative change in conformer populations. Assuming no cooling of conformer populations in the expansion,[21] the relative change in conformer population in heating the nozzle from 100 °C to 400 °C is:

$$\begin{matrix}400\,^\circ\mathrm{C}:\\ \uparrow\\ 100\,^\circ\mathrm{C}:\end{matrix}\ \frac{(anti/gauche)_{400}}{(anti/gauche)_{100}}=\frac{(0.34)}{(0.25)}$$

$$=\text{predicted}\ \frac{[(\mathrm{C-Br})/(\mathrm{C-C})]_{400}}{[\mathrm{C-Br})/(\mathrm{C-C})]_{100}}=1.4 \qquad (4)$$

giving a predicted increase in the C–Br:C–C branching ratio of a factor of 1.4 if C–C fission dominates in the *gauche* conformer and C–Br fission dominates in the *anti* conformer. The experimentally observed change in branching ratio is quite similar:

$$\text{observed}\ \frac{[(\mathrm{C-Br})/(\mathrm{C-C})]_{400}}{[(\mathrm{C-Br})/(\mathrm{C-C})]_{100}}=\frac{(85\%/15\%)}{(78\%/22\%)}=1.6! \qquad (5)$$

The change in thermal conformer populations rely on Durig's[19] calculated 0.5 kcal/mol energy difference between the *gauche* and *anti* conformers; if the actual energy difference were even 0.3 kcal/mol larger, the calculated change in the *anti:gauche* ratio on going from 100 °C to a 400 °C would be near 1.6. Small differences aside, it is clear from the comparison between the predicted and observed change in branching that increasing the fraction of *anti* conformer in the beam and decreasing the fraction of *gauche* conformer results in a corresponding increase in the branching to C–Br fission and decrease in the branching to C–C fission. This result is in accord with the model presented in the previous section (see Fig. 13), in which dissociation from the *anti* conformer accesses regions of the C–C fission reaction coordinate near the conical intersection, where it is nonadiabatically inhibited so cannot compete with C–Br fission, and dissociation from the *gauche* conformer proceeds through regions of the conical intersection where the surfaces are further split from each other, so the C–C dissociation can proceed adiabatically and dominate C–Br fission.[30]

VI. DISCUSSION

This investigation of the competition between C–C and C–Br bond fission in bromoacetone excited in the $^1[n(\mathrm{O}),\pi^*(\mathrm{C{=}O})]$ absorption probed the role of molecular conformation in influencing the probability of adiabatically traversing the conical intersection along the C–C fission reaction coordinate. A detailed discussion of the model for interpreting the experimental results was presented in Sec. V B 2, so we only make a few points here to place the results in a more general context.

We have avoided using the terminology "symmetry forbidden" when describing the lack of C–C fission from the *anti* conformer because, although commonly used, this language obscures the physical reason why a reaction pathway that traverses a conical intersection might be unfavorable. Indeed, the reaction is "symmetry forbidden" only through a singularity point on the potential energy surface; even small zero point bending or torsional motion of the *anti* conformer at the transition state puts amplitude at molecular geometries where the adiabatic correlation goes smoothly from reactants to products. The reason why C–C fission in the *anti* conformer is suppressed is that trajectories that attempt to undergo C–C fission near, but not at, the point of conical intersection sample a region of phase space where the reactant and product electronic configurations are not strongly coupled, and thus the configuration interaction splitting between the upper and lower adiabats is small. Instead of traversing the adiabatic path, along which the electronic wave function changes from $n(\mathrm{O})\pi^*(\mathrm{C{=}O})$ to $\sigma\sigma^*(\mathrm{C-C})$ in character, the dissociative trajectory hops to the upper bound adiabat as it tries to traverse the C–C reaction barrier. Therefore, the mechanism for the forbiddeness is inherently nonadiabatic; it relies on a failure of the Born–Oppenheimer separation of nuclear and electronic motion. Thus a reaction pathway through a conical intersection is not "symmetry forbidden" for most dissociative trajectories, but it is characterized by a high nonadiabatic recrossing probability.

These studies investigated a system which foreshadows a unique class of mode-selective reactions. Whereas the more familiar type of mode-selective chemistry[31] involves preparing the reactants in specific vibrational states which favor accessing one transition state over the other, the preference for C–C fission from the *gauche* conformer relies on accessing regions of phase space, highly nonplanar geometries, where C–C fission can proceed without nonadiabatic recrossing of the reaction barrier. If one could selectively prepare high energy torsional states that extended to the C–C fission barrier region, then the outer turning point of the wave function would sample regions of the barrier where the splitting between adiabats is large and C–C fission would be favored, just as photoexciting the *gauche* conformer does. The geometry dependence of the nonadiabatic branching relies on the fact that the splitting between adiabats varies considerably with the molecular geometry at which the barrier is crossed. Thus, reaction pathways through conical intersections are obvious candidates for this kind of mode-selective chemistry. The results presented here are complementary to earlier work on the photodissociation of ICN and CF_3I through a conical intersection.[32,33] In the work on ICN, photodissociating ICN thermally excited in the bend enhanced the branching to the adiabatic $I(^2P_{3/2})+CN$ products by sampling bent geometries at the conical intersection between the two dissociative surfaces.[33] In linear geometries, only $I(^2P_{1/2})+CN$ would be produced, while at bent geometries the splitting between adiabats at the region of the conical intersection is larger so the adiabatic channel grows in importance. One should note, however, that both the ICN/CF_3I system and *gauche*-bromoacetone have circumvented one critical concern in evaluating the potential generality of mode-selective chemistry. Unlike accessing nonplanar geometries

in bromoacetone with high energy torsional motion, which would involve exciting a zeroth order vibrational state which is unfortunately strongly coupled with other zeroth order rovibrational states of the system, accessing these geometries by exciting from the *gauche* conformer does not necessarily require a breakdown of the RRKM assumption of complete IVR.[34] All it requires is that the region of phase space sampled by the *gauche* conformer be separated from that sampled by the *anti* conformer at the barrier to C–C fission by virtue of the torsional barrier in the excited state.

ACKNOWLEDGMENTS

This work was supported by the National Science Foundation, currently under renewal Grant No. CHE-9307500. The collaboration with M.M.F. was supported by a Summer Faculty Research Fellowship, a supplement to our Grant No. 22218-AC6 from the donors of The Petroleum Research Fund, administered by the ACS, and by the Rosalyn R. Schwartz Lectureship. L.J.B. gratefully acknowledges the support of a Camille and Henry Dreyfus Foundation Teacher-Scholar Award and an Alfred P. Sloan Research Fellowship.

[1] The development of statistical transition state theories is reviewed by K. J. Laidler and M. C. King, J. Phys. Chem. **87**, 2657 (1983).

[2] The current status of statistical transition state theory is reviewed by D. G. Truhlar, W. L. Hase, and J. T. Hynes, J. Phys. Chem. **87**, 2664 (1983).

[3] P. J. Robinson and K. A. Holbrook, *Unimolecular Reactions* (Wiley-Interscience, London, 1972).

[4] Recent formulations of transition state theory to account for nonadiabatic effects include: A. J. Marks and D. L. Thompson, J. Chem. Phys. **96**, 1911 (1992) and pioneering work referenced within, and S. A. Schofield and P. G. Wolynes, J. Chem. Phys. **100**, 350 (1994).

[5] See, for example, extensive references on pp. 296–299 in R. D. Levine and R. B. Bernstein, *Molecular Reaction Dynamics and Chemical Reactivity* (Oxford University, New York, 1987), Sec. 5.6.

[6] M. Born and R. Oppenheimer, Ann. Phys. **84**, 457 (1927). For one of the best early reviews of nonadiabatic molecular collisions, see J. C. Tully, in *Dynamics of Molecular Collisions Pt. B*, edited by W. H. Miller (Plenum, New York, 1976), p. 217.

[7] (a) M. D. Person, P. W. Kash, S. A. Schofield, and L. J. Butler, J. Chem. Phys. **95**, 3843 (1991); (b) M. D. Person, P. W. Kash, and L. J. Butler, J. Chem. Phys. **97**, 355 (1992).

[8] P. W. Kash, G. C. G. Waschewsky, L. J. Butler, and M. M. Francl, J. Chem. Phys. **99**, 4479 (1993).

[9] See, for example, the qualitative description of the change in electronic configuration across a barrier in R. B. Woodward and R. Hoffmann, *The Conservation of Orbital Symmetry* (Chemie, Weinheim/Bergstrasse, 1970) and in D. M. Silver, J. Am. Chem. Soc. **96**, 5959 (1974).

[10] For a brief but helpful qualitative introduction to nonadiabatic surface hopping, see J. Michl and V. Bonačić–Koutecký, *Electronic Aspects of Organic Photochemistry* (Wiley, New York, 1990), p. 20.

[11] The universal detector was introduced by Y. T. Lee, J. D. McDonald, P. R. LeBreton, and D. R. Herschbach, Rev. Sci. Instrum. **40**, 1402 (1969).

[12] For details, see M. D. Person, Ph.D. thesis, Department of Chemistry, University of Chicago, 1991.

[13] GAUSSIAN 92, Revision C, M. J. Frisch, G. W. Trucks, M. Head-Gordon, P. M. W. Gill, M. W. Wong, J. B. Foresman, B. G. Johnson, H. B. Schlegel, M. A. Robb, E. S. Replogle, R. Gomperts, J. L. Andres, K. Raghavachari, J. S. Binkley, C. Gonzalez, R. L. Martin, D. J. Fox, D. J. Defrees, J. Baker, J. J. P. Stewart, and J. A. Pople (Gaussian, Inc., Pittsburgh, PA, 1992).

[14] The peak of the absorption band is reported in K. Yates, S. L. Klemenko, and I. G. Csizmadia, Spectrochim. Acta Part A **25**, 765 (1969).

[15] Although the data on the two systems are taken at different photon energies, we still use the same $P(E_T)$ for C–Br fission upon $^1[n(O), \pi^*(C{=}O)]$ excitation because the kinetic energy release for dissociation along a reaction coordinate with an exit barrier should be relatively insensitive to photon energy. See, for example, the close comparison of the kinetic energy release for 200 and 218 nm excitation energies in C–O fission in acetic acid reported by S. S. Hunnicutt, L. D. Waits, and J. A. Guest, J. Phys. Chem. **95**, 562 (1991).

[16] P. W. Kash, G. C. G. Waschewsky, and L. J. Butler, J. Chem. Phys. **100**, 4017 (1994).

[17] Both the bromoacetone and chloroacetone conformers have historically been named in a nonstandard way. The conformer designated as "*trans*" or "*anti*" in this and previous papers should, in correct nomenclature, be called *s-cis*, as the dihedral angle between the C–Cl(Br) and the C=O bond is zero and the Cl or Br and O atoms, having the highest atomic numbers, should determine the groups to which the geometry refers. However, we retain the nonstandard name of *trans* or *anti* for this conformer in order to remain consistent with several earlier studies beginning with the first study of rotational isomerism of chloroacetone, see S. Mizushima, T. Shimanouchi, T. Miyazawa, I. Ichishima, K. Kuratani, I. Nakagawa, and N. Shido, J. Chem. Phys. **21**, 815 (1953). In that work, the authors compared their results to XH_2C–COY systems (X,Y=halogens), so they called the conformer of chloroacetone in which the Cl is *s-cis* to the O atom but *trans* to the CH_3 group the *"trans"*, rather than the more correct name of *s-cis*. Later papers retained this nonstandard designation for both chloroacetone and bromoacetone, and added the name *gauche* (or near *cis*) to the other conformer, where the Cl or Br atom is near *cis* to the CH_3 group (not the O atom).

[18] R. N. Zare, Mol. Photochem. **4**, 1 (1972).

[19] Using the calculated equilibrium geometries in J. R. Durig, J. Lin, and H. V. Phan, J.Rama Spectrosc. **23**, 253 (1992).

[20] The expression $\beta=2P_2(\cos\alpha)$ is given in G. E. Busch and K. R. Wilson, J. Chem. Phys. **56**, 3638 (1972); S. C. Yang and R. Bersohn, *ibid* **61**, 4400 (1974).

[21] Conformation relaxation in supersonic expansions with He as the carrier gas is shown to be minimal (for molecules in which the barrier between conformers is greater than 400 cm^{-1}) by R. S. Ruoff, T. D. Klots, T. Emilsson, and H. S. Gutowsky, J. Chem. Phys. **93**, 3142 (1990).

[22] This assumes that the dissociation quantum yield and absorption spectrum is insensitive to conformer at this wavelength. A further measurement supports this in Sec. V B 3.

[23] Further details on our calculation may be found in R. Morss, B. A. honors thesis, Department of Chemistry, University of Chicago, 1993.

[24] For a point of reference, the shortest C=O bond length of 1.182 Å at which surfaces were calculated in *anti*-bromoacetone and 1.186 Å in *gauche*-bromoacetone is the equilibrium C=O bond length as reported by Durig and co-workers.[19] The C=O bond length of 1.282 Å in *anti*-bromoacetone and 1.280 Å in *gauche*-bromoacetone are near the equilibrium bond length we calculated based on the minimum in the C=O ground state potential from our CISD calculations.[23] The C=O bond lengths of 1.392 Å in *anti*-bromoacetone and 1.380 Å in *gauche*-bromoacetone are near our calculated equilibrium C=O bond length in the $^1n(O),\pi^*(C{=}O)$ excited electronic state.

[25] T. H. Lowry and K. S. Richardson, *Mechanism and Theory in Organic Chemistry* (Harper & Row, New York, 1987), p. 1041.

[26] Although *a*-cleavage is usually assumed to occur via internal conversion or intersystem crossing, an excited state singlet mechanism has been reported in Ref. 28 and we note that the $^1A'$, $^1\sigma\sigma$, asymptotic limit of the ground state must have a corresponding antibonding $^1\sigma\sigma^*$ state that should correlate adiabatically with the lowest $^1A''$,$^1n\pi^*$, state in geometries where the plane of symmetry is broken.

[27] See M. Reinsch and M. Klessinger, J. Phys. Org. Chem. **3**, 81 (1990), and extensive references within.

[28] N. C. Yang and E. D. Feit, J. Am. Chem. Soc. **90**, 504 (1968).

[29] We use the words planar and nonplanar here to refer to molecular geometries that do or do not have a plane of symmetry. Of course, although all the heavy atoms are in a plane in "planar" geometries, the H atoms are not.

[30] We should note that for reactions without a large exit barrier (if, for instance, the mechanism were via internal conversion to the ground

state) an increase in the internal energy in unimolecular transition state theory would normally increase the branching to fission of the stronger C–C bond (with a higher barrier energy) over the C–Br bond, not the reverse, (although weak bond fission would still dominate) so one cannot invoke this simple interpretation of the results.

[31] See, for example, the mode selective H+HOD reaction studied by (a) G. C. Schatz, M. C. Colton, and J. L. Grant, J. Phys. Chem. **88**, 2971 (1984); (b) A. Sinha, M. C. Hsiao, and F. F. Crim, J. Chem. Phys. **92**, 6333 (1991) and *ibid*, **94**, 4928 (1991); (c) M. J. Bronikowski, W. R. Simpson, B. Girard, and R. N. Zare, J. Chem. Phys. **95**, 8647 (1991) and *ibid*, J. Phys. Chem. **97**, 2194, 2204 (1993).

[32] M. D. Person, P. W. Kash, and L. J. Butler, J. Chem. Phys. **94**, 2557 (1991).

[33] P. W. Kash and L. J. Butler, J.Chem. Phys. **96**, 8923 (1992).

[34] For an excellent review of intramolecular vibrational relaxation (IVR) and a zeroth order vibrational state description as relevant to statistical processes, see K. F. Freed and A. Nitzan, in *Energy Storage and Redistribution in Molecules*, edited by J. Hinze (Plenum, New York, 1983), p. 467.